Structure and Mechanism of Inosine Monophosphate Dehydrogenase in Complex with the Immunosuppressant Mycophenolic Acid

Michael D. Sintchak, Mark A. Fleming, Olga Futer, Scott A. Raybuck, Stephen P. Chambers, Paul R. Caron, Mark A. Murcko, and Keith P. Wilson
Vertex Pharmaceuticals Incorporated
40 Allston Street
Cambridge, Massachusetts 02139-4211

Summary

The structure of inosine-5′-monophosphate dehydrogenase (IMPDH) in complex with IMP and mycophenolic acid (MPA) has been determined by X-ray diffraction. IMPDH plays a central role in B and T lymphocyte replication. MPA is a potent IMPDH inhibitor and the active metabolite of an immunosuppressive drug recently approved for the treatment of allograft rejection. IMPDH comprises two domains: a core domain, which is an α/β barrel and contains the active site, and a flanking domain. The complex, in combination with mutagenesis and kinetic data, provides a structural basis for understanding the mechanism of IMPDH activity and indicates that MPA inhibits IMPDH by acting as a replacement for the nicotinamide portion of the nicotinamide adenine dinucleotide cofactor and a catalytic water molecule.

Introduction

Proliferating B and T lymphocytes are singularly dependent on the de novo pathway, rather than the salvage pathway, for purine biosynthesis (Allison et al., 1977). Modulation of this metabolic pathway, with broad therapeutic potential, involves the pharmaceutical inhibition of inosine-5′-monophosphate dehydrogenase (IMPDH; EC 1.1.1.205).

IMPDH catalyzes the nicotinamide adenine dinucleotide (NAD)-dependent oxidation of inosine-5′-monophosphate (IMP) to xanthosine-5′-monophosphate (XMP), which is the committed step in de novo guanosine nucleotide biosynthesis (Crabtree and Henderson, 1971; Snyder et al., 1972; Jackson et al., 1975; Weber, 1983). This reaction is particularly important to B and T lymphocytes, which depend on IMPDH activity to generate the guanosine nucleotide levels needed to initiate a proliferative response to mitogen or antigen (Allison et al., 1975). Increased IMPDH activity has also been observed in rapidly proliferating human leukemic cell lines, solid tumor tissues, and other replicating cell types (Natsumeda et al., 1988; Collart and Hubermann, 1990; Konno et al., 1991; Nagai et al., 1991, 1992; Collart et al., 1992; Nakamura et al., 1992; Senda and Natsumeda, 1994). Thus, IMPDH is a target for cancer as well as immunosuppressive chemotherapy (Jackson et al., 1975).

Isoforms (2) of human IMPDH, designated type I and type II, have been identified (Collart and Hubermann, 1988; Natsumeda et al., 1990). Each contains 514 amino acids, and they share 84% sequence identity. IMPDH is also found in bacteria and protozoa, and these forms share 30%–40% sequence identity with the human enzyme (Natsumeda and Carr, 1993). Regardless of species, native IMPDHs exist as homotetramers with subunit molecular masses in the 56–58 kDa range (Carr et al., 1993) and follow an ordered Bi–Bi reaction sequence, where IMP binding precedes that of NAD, and reduced nicotinamide adenine dinucleotide (NADH) is released prior to XMP (Holmes et al., 1974; Carr et al., 1993). This mechanism is different from that of most other known NAD-dependent dehydrogenases, which have either a random order of substrate addition or require that NAD bind before substrate.

Mycophenolic acid (MPA; Figure 1) was discovered in 1896 as a fermentation product of several Penicillium species (Gosio, 1896) and is a potent uncompetitive reversible inhibitor of IMPDH (Franklin and Cooke, 1969). MPA binds to IMPDH after NADH is released but before XMP is produced (Hedstrom and Wang, 1990; Link and Straub, 1996). Reported K_i values for human type II IMPDH are 6–10 nM (Carr et al., 1993; Hager et al., 1995), and estimates for the human type I enzyme vary from 11 nM (Hager et al., 1995) to 33–37 nM (Carr et al., 1993). It is not clear which isoform is the more important therapeutic target. Early reports indicated that only IMPDH type II was up-regulated during proliferation of lymphatic and leukemic cell lines (Konno et al., 1991; Nagai et al., 1991, 1992; Collart et al., 1992), but recent studies in T cells revealed similar increases in the mRNA levels of both isoforms following mitogenic stimulation (Dayton et al., 1994). Mycophenolate mofetil, the morpholinoethyl ester prodrug of MPA, was recently approved for the prevention of acute allograft rejection following kidney transplant (Shaw et al., 1995; Sollinger, 1995), which demonstrates the importance of IMPDH in the cellular immune response.

We report the X-ray crystal structure of Chinese hamster (Cricetulus griseus) IMPDH in complex with IMP and MPA at 2.6 Å resolution (Table 1). We have confirmed that human type II and Chinese hamster IMPDH, which differ by only six amino acids (Collart and Hubermann, 1988), have similar enzymatic characteristics (data not shown) and are both strongly inhibited by MPA. The structure, in combination with kinetic and mutagenesis data, better defines the enzymatic mechanism of IMPDH and reveals the exact nature of the inhibition of IMPDH by MPA.

Results

Global Fold and Tetramer Contacts of IMPDH

Each IMPDH monomer consists of two domains (Figure 2). The larger domain had approximate dimensions of 40 × 40 × 50 Å and formed an α/β barrel. This finding is consistent with structure predictions based on primary sequence (Bork et al., 1995). The active-site loop (residues 325–342) starts just after strand 6, and like all barrel enzymes examined to date, resides at the C-terminal end of the barrel β strands. Comparisons of this domain

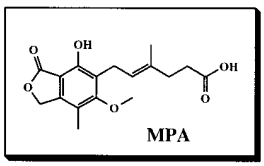

IC_{50} (μM)

0.020

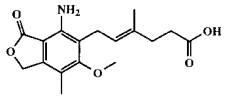

IC_{50} (μM)

0.154

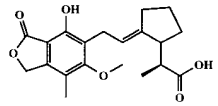

0.008

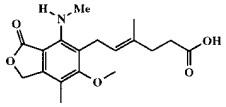

48

Figure 1. MPA and MPA Analogs

Chemical structure of MPA and three analogs, along with IC_{50} values as reported in Syntex patents (Sjogen, 1995; Artis et al., 1995). The IC_{50} data are based on an in vitro assay that measures the formation of NADH by UV/VIS spectroscopy at 340 nm.

of IMPDH with proteins in the Protein Data Bank identified glycolate oxidase, tryptophan synthase, and indole-3-glycerol phosphate synthase as enzymes with similar folds and C-terminal phosphate-binding sites. The closest known structural homolog to IMPDH is glycolate oxidase, with a backbone root-mean-square deviation of 1.49 Å over 172 residues. The sequence of glycolate oxidase also shows local homology to that of IMPDH, with 40% identity over 40 amino acids in the region surrounding the phosphate-binding site.

The smaller flanking domain (designated subdomain here) includes residues 110–244 and is inserted between the second α helix and third β strand of the barrel. The subdomain has rough dimensions of 20 × 20 × 40 Å and protrudes from the N-terminal side of the barrel core (Figure 2). IMPDH is unique among α/β barrels in this regard. A comparison of IMPDH to aligned protein structures in the FSSP database (Holm and Sander, 1996) located only 15 amino acids as the next largest insertion at the N-terminal end of any α/β barrel. In addition, sequence comparisons identified GMP reductase as the closest IMPDH homolog, but the subdomain residues are absent in this enzyme (Andrews and Guest, 1988). The sequence and fold of the subdomain also

Table 1. Statistics for Data Collection and Structure Determination

Data Collection	Native (imp + mpa)	K_2WO_4	$(NH)_2WS_4$	PCMBS 1	PCMBS 2	PbCl	$EuCl_3$	tet-HgCl furan	bis-Hg bi-thiophene	bis-Hg benzofuran
Resolution (Å)	2.6	3.5	4.5	4.0	4.0	4.0	3.0	3.2	2.0	2.9
Observations	123,246	45,765	10,610	27,429	40,754	19,998	139,573	113,378	113,758	114,000
Unique Reflections	37,492	16,341	5,363	10,222	10,719	9,792	25,060	19,805	27,766	27,230
Completeness (%)	93	93	64	86	89	82	99	87	92	93
R_{sym}	5.2	7.4	13.4	6.7	8.7	8.3	10.7	9.1	6.6	6.6
MIR Phasing										
Resolution (Å)	4.0	4.0	4.0	4.0	4.0	4.0	4.0	4.0	4.0	4.0
R_{iso}		5.9	11.7	13.6	26.0	8.1	14.2	18.5	11.4	14.3
number of sites		3	4	6	11	1	3	5	3	6
R_{cullis}		0.73	0.76	0.68	0.54	0.77	0.69	0.60	0.57	0.58
Phasing power		0.90	0.52	0.80	1.41	0.49	0.76	2.03	2.71	2.75
Mean overall FOM	0.79									

Refinement	
Resolution	8.0–2.6
R_{cryst} (%)	21.7
R_{free} (%)	28.5
Nonhydrogen atoms	6,101
Water molecules	202
root-mean-square deviation	
Bond lengths (Å)	0.007
Bond angles (°)	1.627
Dihedrals (°)	22.27
Impropers (°)	1.269

For definitions, see Blundell and Johnson (1976).

(*Figure 2 legend continued*)

not visible in electron density maps are marked "???." The flap (residues 400–450) between strand β8 and helix α8 includes strands βJ–βN and helix αE. Residue assignments for the strands and helices that form the α/β barrel are as follows: β1, residues 65–68; α1, 76–85; β2, 88–91; α2, 98–109; β3, 245–250; α3, 256–266; β4, 270–274; α4, 281–293; β5, 298–302; α5, 307–316; β6, 320–324; α6, 343–355; β7, 360–364; α7, 370–378; β8, 382–386; and α8, 456–469. Residue assignments for the remaining secondary structural elements are as follows: βA, residues 18–19; βB, 35–38; βC, 40–42; βD, 53–55; βE, 59–61; βF, 114–116; βG, 186–189; βH, 206–212; βI, 220–223; βJ, 400–402; βK, 406–409; βL, 411–413; βM, 438–440; βN, 443–448; βO, 489–492; βP, 509–513; αA, 21–23; αB, 194–200; αC, 225–232; αD, 333–337; αE, 416–420; αF, 476–484; and αG, 495–501.

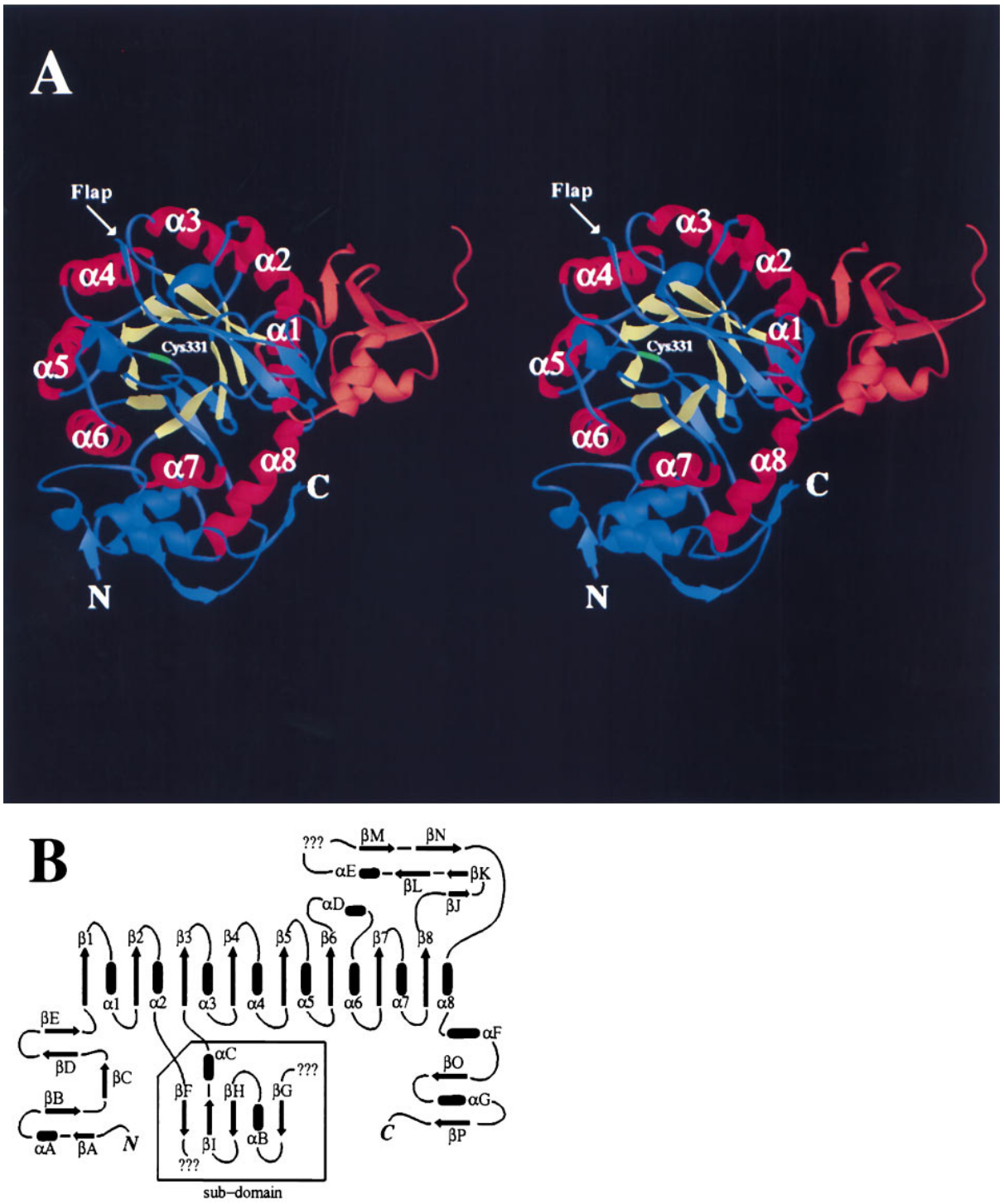

Figure 2. Structure and Topology of IMPDH

(A) Stereo ribbon diagram (Carson, 1991) of IMPDH. The structure is viewed from the C-terminal end of the β strands (yellow) that form the α/β barrel. The α helices (red) on the outside of the barrel are labeled α1–α8. The portion of the subdomain (orange) that is ordered is shown. Cys-331 (green) is labeled and sits over one end of the barrel. An arrow marks the location of the flap (residues 400–450) that, together with the active-site loop, helps form the active-site pocket.

(B) Topology diagram of the IMPDH fold. Secondary structure was assigned using the Kabsch and Sander algorithm (Kabsch and Sander, 1983), along with visual inspection. The β strands and α helices that form the α/β barrel core are labeled β1–β8 and α1–α8. The strands and helices that are not part of the barrel are labeled βA–βP and αA–αG. Cys-331 is located on the loop between strand β6 and helix αD. The subdomain starts after helix α2 and ends at strand β3 and includes strands βF–βI and helices αB and αC. Parts of the structure that were

(*Figure 2 legend continued on previous page*)

appeared to be novel, as no corresponding matches could be found. The function of the subdomain in IMPDH is not known, and the structure reveals that this domain is 35 Å away from the active site and is relatively disordered (Figure 2). There is considerable variation in the size and sequence of this region among IMPDHs from different species, including Borrelia burgdorferi IMPDH (Genbank accession number U13372), which lacks most of the subdomain residues. A deletion mutant that replaces the entire subdomain in human type II IMPDH with a short peptide linker has been made, and the truncated enzyme is fully active in vitro (our unpublished data).

IMPDH is active in solution and crystallizes as a tetramer, and extensive contacts between barrels of adjacent monomers helped stabilize this form (Figure 3). Most of the tetramer-related contacts arose from residues near the N- and C-terminus of one subunit that contacted amino acids that were part of or near the active site of an adjacent subunit. These interactions may help stabilize the active-site conformation. The subdomain made no tetramer contacts.

The Active Site

We have determined the structure of IMPDH in complex with MPA and an IMP reaction intermediate that is generated during substrate turnover. In this inhibited state, hydride transfer and NADH release has occurred, but XMP has not been produced (Link and Straub, 1996; Fleming et al., 1996). Thus, MPA and an IMP intermediate are bound in the active site simultaneously. This observation is consistent with the uncompetitive inhibition of IMPDH by MPA. The electron density in the active site clearly shows that a covalent bond is formed between the C2 carbon of IMP and the sulfur atom of Cys-331 (Figure 4) to yield an oxidized IMP thioimidate intermediate (XMP*). Cys-331 has also been shown to form a covalent bond with ^{14}C8-IMP when NAD is present (Huete-Perez et al., 1995; Link and Straub, 1996). In addition, Cys-331 forms a covalent bond to 6-Cl IMP and EICARMP, compounds which irreversibly inactivate IMPDH (Antonino et al., 1994; Wang et al., 1996). Together, these observations establish an important role for this residue in catalysis.

In addition to the covalent bond to Cys-331, many other interactions between XMP* and the enzyme were observed (Figure 4). The phosphate moiety forms hydrogen bonds with four backbone amide nitrogen atoms and the side-chain hydroxyl groups of Tyr-411 and Ser-329. Tyr-411 is located on one of a pair of β strands (residues 406–413 and 443–448) that are part of a flap (residues 400–450) that makes three hydrogen bonds with the hypoxanthine ring. Together, these interactions may help order this region of IMPDH. This hypothesis is supported by proteolysis experiments that show that IMPDH is protected from cleavage by elastase after residues 437 and 440 when IMP is present (Nimmesgern et al., submitted). The ribose ring, which adopts a C3′-*endo* conformation, also contributes significantly to binding. The structure shows that the O2′ and O3′ hydroxyl groups form a hydrogen-bonding network to Ser-68 and Asp-364. Van der Waals contacts between XMP*, Met-70, and Ile-330 were also observed.

MPA is a potent (K_i = 11 nM) uncompetitive inhibitor of Chinese hamster IMPDH, and the structure reveals many interactions between MPA and IMPDH active-site residues (Figure 4). One face of the bicyclic ring system is stacked on the XMP* hypoxanthine ring, while the other makes contact with the main-chain atoms of Ser-276. Together, the hexenoic acid tail, methyl substituent, and methoxy group of MPA make van der Waals contacts with the side-chain atoms of Asp-274, Ser-275, Ser-276, Asn-303, Arg-322, and Gln-441. Hydrogen bonds (6) between the drug and IMPDH were also observed. These included hydrogen bonds between the O2 lactone oxygen and the amide nitrogen of Gly-326, and the C1 carbonyl oxygen and hydroxyl group of Thr-333. The hexenoic acid tail of MPA adopts a bent conformation, unlike the extended conformation seen in the nuclear magnetic resonance studies (Makara et al., 1996) and crystal structure of free MPA (Harrison et al., 1972). This conformation allows the carboxylate group to form hydrogen bonds with the amide nitrogen and side-chain hydroxyl groups of Ser-276. Additionally, the C7 phenolic oxygen forms hydrogen bonds to the side-chain hydroxyl group of Thr-333 and the side-chain amide of Gln-441.

Mutational and Kinetic Analysis of the Active Site

We generated a series of mutants to explore the roles of human type II IMPDH active-site residues in catalysis and inhibitor binding (Figure 5). Knowledge of the three-dimensional structure permitted rationalization of the observed phenotype. Mutation of either Cys-331 or Asp-364 to Ala effectively abolished IMPDH activity relative to wild type. The crystal structure revealed that Cys-331 formed a covalent bond to XMP*, confirming its role in catalysis, while the side chain of Asp-364 formed a hydrogen bond to the ribose moiety of XMP*. Changing Ser-329 to Ala reduced enzyme activity to 13% of the wild-type level. This side chain formed a hydrogen bond to the phosphate of XMP*. Residues that made direct contact with MPA were also modified. Substituting Thr-333 with Ile and Gln-441 with Ala increased the K_i apparent of MPA 300-fold and 25-fold, respectively. The Thr-333→Ile mutation is of particular interest, since it has been observed in murine blastoma cells selected for 10,000-fold increased resistance to MPA (Hodges, 1989; Lightfoot and Snyder, 1994). The crystal structure showed a hydrogen bond network between Thr-333, Gln-441, and MPA, with the phenolic oxygen in particularly good hydrogen bonding distance and geometry with the side-chain hydroxyl of Thr-333 (see Figure 4). The carboxylate group of the hexenoic acid tail of MPA formed two hydrogen bonds with Ser-276. Mutating this residue to Ala disrupted this interaction and led to a 7-fold increase in K_i apparent. In contrast, mutations of other active-site residues, such as Ser-275, Ser-327, and Gln-368, had little effect on catalytic activity or drug inhibition. The structure indicates that these residues do not contact substrate or inhibitor directly.

IMPDH Dependence on Potassium

Kinetic experiments with human IMPDH reveal that, although IMP can bind to the enzyme in the absence of

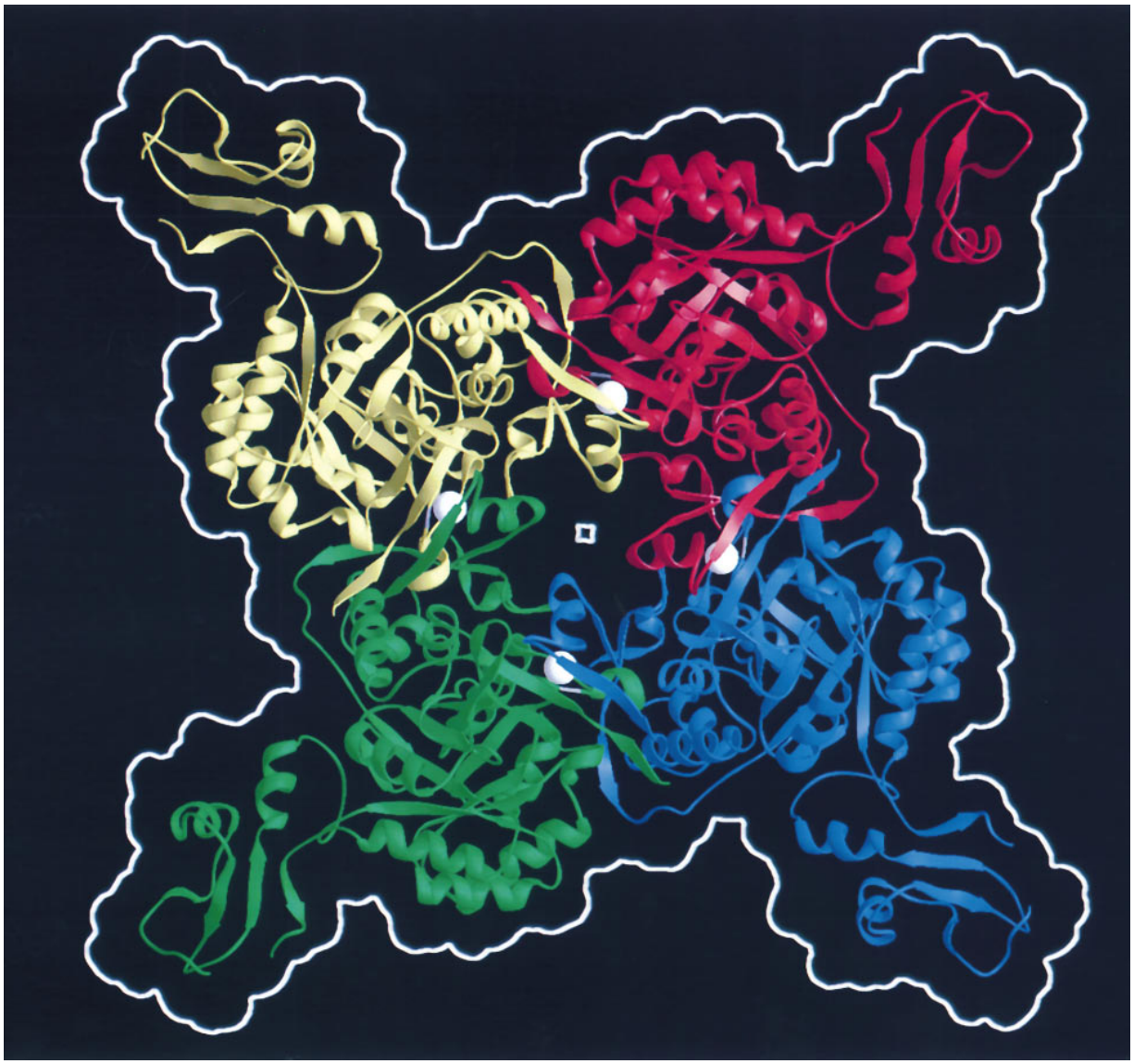

Figure 3. Structure of the IMPDH Tetramer

Ribbon drawing (Carson, 1991) of the IMPDH tetramer, viewed down the crystallographic 4-fold axis. Each IMPDH monomer is colored differently. The white outline represents the solvent-accessible surface. Most of the tetramer-related contacts are made between adjacent barrels, and the surface area buried at each subunit interface is approximately 4000 Å^2. Bound potassium ions (white spheres) are seen adjacent to Cys-331 at each subunit interface. Several other contacts are noteworthy. Residues 41–43 form a β strand parallel with residues 279–281 in an adjacent subunit. Residues 502–503 make van der Waals contact with Cys-331 in an adjacent subunit. Residues 507–510 form an antiparallel β strand with residues 444–447 of the active-site flap of an adjacent subunit, and these two strands can be seen above the potassium ions.

potassium, this ion is required for the reaction to proceed (Xiang et al., 1996). The structure explains this observation. We observed a large peak in difference electron-density maps that was surrounded by a water molecule and five main-chain carbonyl oxygens, including that of Cys-331 (data not shown). The average distance of the peak center to each of the surrounding ligands was 3.1 Å, and the peak was hexagonally coordinated. The nature and positioning of the ligands suggested a potassium-binding site. Thus, potassium may organize protein conformation around the active site and could help position Cys-331 for catalysis. In addition, three of the carbonyl oxygen ligands resided on residues near the C-terminus of an adjacent IMPDH subunit, suggesting that potassium may also stabilize the tetramer form of IMPDH (see Figure 3).

Discussion

Proliferating B and T lymphocytes are singularly dependent on the de novo, as opposed to salvage, pathway for purine biosynthesis. Inhibitors of IMPDH, which catalyzes the rate-limiting step in the de novo synthesis of guanosine nucleotides, have been shown to have a strong immunosuppressive effect. One such compound is MPA. The ternary complex described here reveals

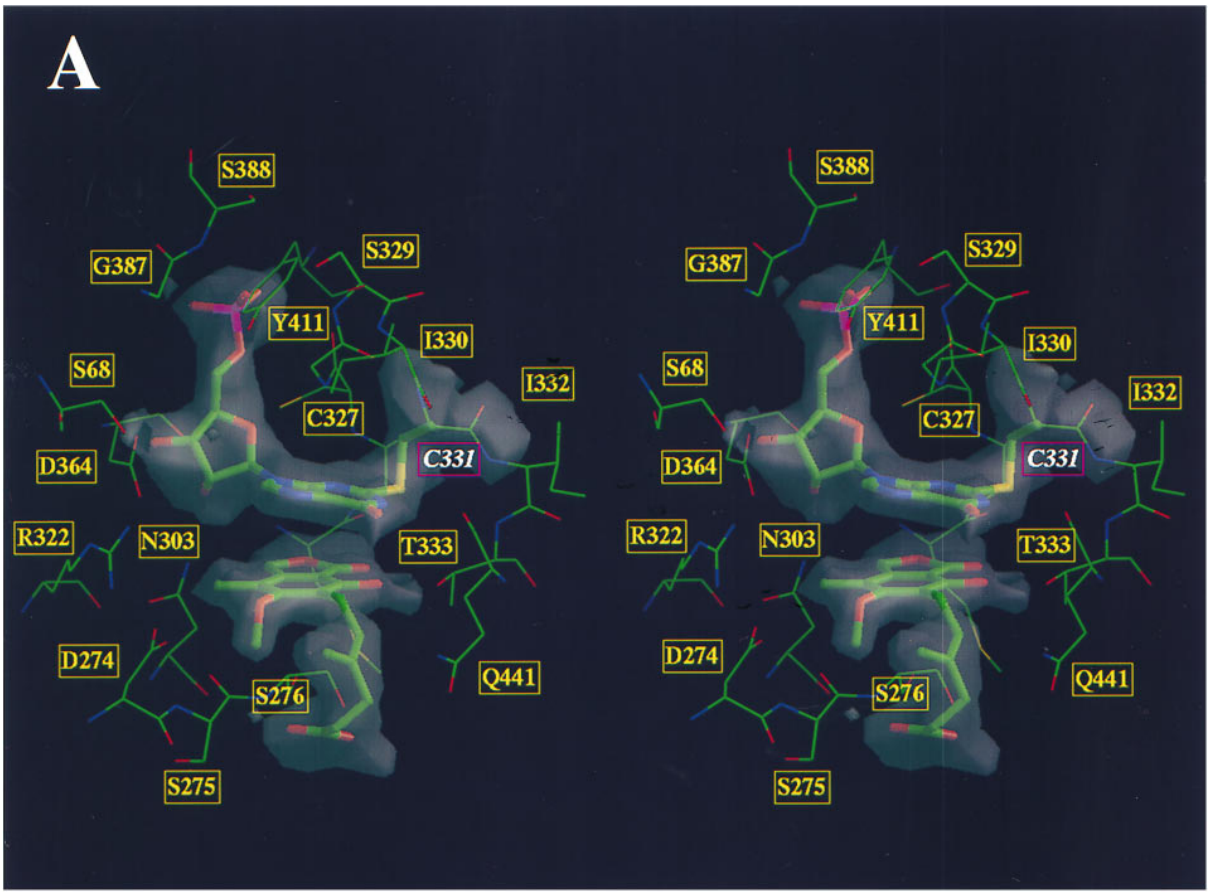

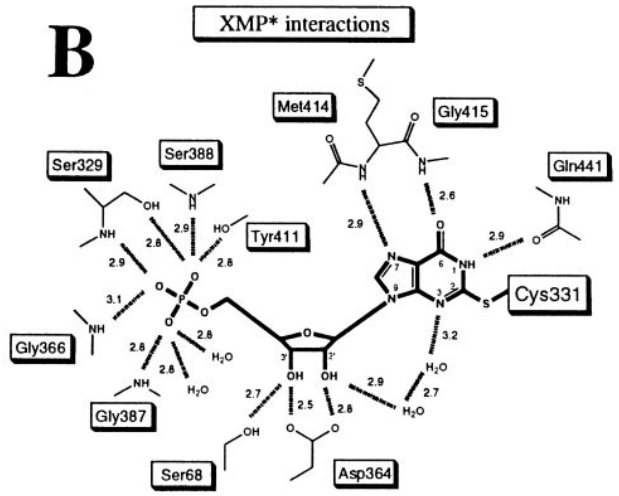

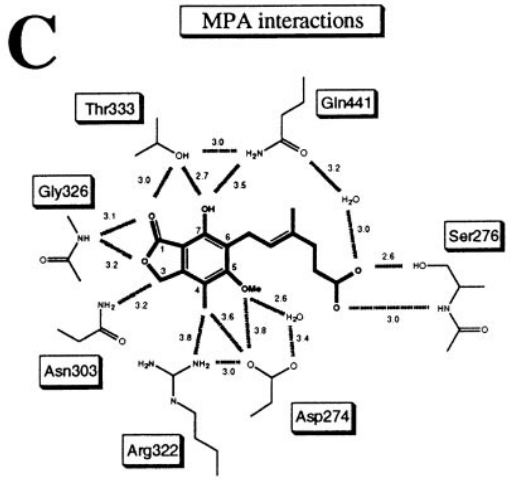

Figure 4. IMPDH Active-Site Electron Density and Interactions

(A) Stereo view of the IMPDH active-site electron density (Carson, 1991). Refined coordinates of the IMP thioimidate intermediate and MPA are shown in thick bonds superimposed on the SigmaA-weighted (Read, 1986) $2F_{obs}–F_{calc}$ electron density contoured at 2.0 σ. Carbon atoms are green, nitrogen atoms blue, oxygen red, sulfur yellow, and phosphorous purple. The hypoxanthine ring makes a covalent bond to the sulfur of Cys-331. Side chains that interact with substrate or inhibitor to form the active-site pocket are shown using thin bonds. These interactions should also apply to the human type II form of IMPDH. There are only six differences in amino acid sequence between Chinese hamster and human type II IMPDH (R173C, N215D, L265Q, M290I, E292D, and C327S). These side chains are all at least 15 Å away from the active site, except C327S, which is a conservative mutation and points away from the active-site pocket.

(B) Schematic representation of the XMP*–IMPDH interactions. There is a covalent bond between the sulfur atom of Cys-331 and the C2 carbon of the hypoxanthine ring.

(C) Schematic representation of the MPA–IMPDH interactions. All proximal water molecules observed in electron density difference maps are labeled "H_2O." All distances pertain to nonhydrogen atoms.

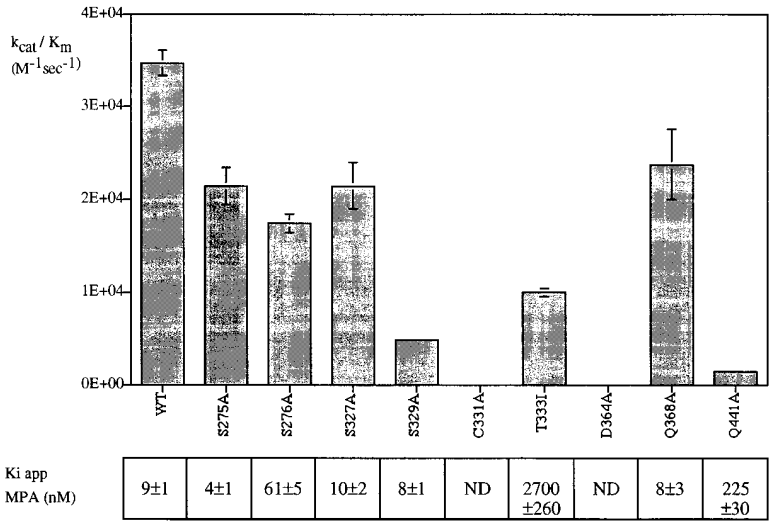

Figure 5. Mutational and Kinetic Analysis of the Active Site

(A) Specific activity of IMPDH mutants for IMP substrate. Second-order rate constants (k cat/Km, $M^{-1}sec^{-1}$) were calculated from IMP titration data at 400 mM NAD concentration, obtained by monitoring the rate of NADH production at 340 nm at 37°C. We have confirmed that 400 mM NAD is saturating for all mutants depicted here.

(B) Inhibition of mutant IMPDH proteins by MPA. K_i apparent values for MPA were obtained from the rate versus inhibitor data of IMPDH mutants at saturating IMP and NAD concentrations. The data were fit to the equation for tight-binding uncompetitive inhibition using the program KineTic 3.0 (Morrison, 1969).

much about the structure and mechanism of IMPDH and provides atomic level details of an immunosuppressant inhibiting its cellular target.

Enzymatic Mechanism of IMPDH and Inhibition by MPA

The IMPDH catalyzed oxidation of IMP results in transfer of hydrogen to the nicotinamide ring of NAD, forming NADH and XMP. Since direct transfer of the hydride is energetically unfavorable, two mechanisms involving activation of IMP at the inosine C2 position have been proposed (Hedstrom and Wang, 1990). In the first mechanism, water, aided by an active-site base to provide OH^- attack, is added in an initial step at C2. Hydride transfer to NAD then occurs from the tetrahedral intermediate thus formed, producing the enol tautomer of XMP. In the second mechanism, nucleophilic attack on IMP occurs from an active-site cysteine thiol. This is followed by hydride transfer to NAD to yield a covalently bound thioimidate intermediate that is hydrolyzed to XMP in a subsequent step. The crystal structure, in combination with recent results that also demonstrate the formation of an IMPDH–substrate covalent adduct (Huete-Perez et al., 1995; Link and Straub, 1996), strongly supports the second mechanism. The direct observation of the covalently bound thioimidate as the oxidized IMP intermediate confirms that enzyme-catalyzed oxidation of IMP occurs via attack of Cys-331 at the C2 position and excludes a general base mechanism where water is added to the inosine ring in an early step.

Other aspects of the IMPDH catalyzed reaction can be addressed with the crystal structure. Although the MPA inhibited complex does not contain NAD or NADH, a combination of structural and chemical evidence allows the nicotinamide ring to be modeled into the active site. The nicotinamide ring must be oriented to allow hydride transfer from the C2 position of IMP to the C4 position of NAD. Further, hydride transfer occurs more readily if the nicotinamide and hypoxanthine rings are nearly parallel (Wu et al., 1995), consistent with the favorable interactions provided by stacking between the nicotinamide ring and the bound substrate, and as observed in the structures of glutathione reductase and NADH peroxidase. It is also known that hydride transfer occurs on the β face of NAD (Cooney et al., 1987). If no large conformational changes occur between the time NADH leaves and MPA binds, these structural considerations support an earlier prediction (Hedstrom and Wang, 1990) that during hydride transfer the nicotinamide of NAD occupies a position similar to the 6,5 ring system of MPA. In this orientation, the nicotinamide amide moiety would form hydrogen bonds with Gly-324, Thr 333, Gly-326, and Asn-303.

The structure of the inhibited complex also indicates that the phenolic hydroxyl group of MPA, which forms hydrogen bonds to Thr-333 and Gln-441, may be a replacement for the catalytic water that hydrolyzes the thioimidate intermediate to produce XMP. In the absence of MPA, a water molecule in the vicinity of the MPA hydroxyl would be stabilized by hydrogen bonds with Thr-333 and Gln-441 and would be properly positioned for nucleophilic attack at the C2 carbon of the thioimidate intermediate. Therefore, structural features of the bound orientation of MPA indicate that it is both a nicotinamide ring and a catalytic water mimic. This hypothesis is consistent with a report that des-hydroxy-MPA is at least 1000-fold less potent in a cellular assay than MPA (Or et al., 1995, Am. Chem. Soc., poster). It has also been shown that the presence of a hydroxyl group which is able to mimic a catalytic water molecule can lead to as much as a 10 kcal/mol improvement in binding (Wolfendon and Kati, 1991). Additional active-site mutants, coupled with substrate and MPA analog studies underway, will test these hypotheses.

Inhibition of IMPDH by Analogs of MPA

The crystal structure of the MPA–inhibited complex helps to explain some of the known structure–activity data for analogs of MPA (Figure 1), which also bind as uncompetitive inhibitors (data not shown). Replacement of the phenolic hydroxyl by amino leads to an 8-fold reduction in potency (Sjogen, 1995). The structure indicates that this change would result in the loss of one

hydrogen bond in the network between MPA, Thr-333, and Gln-441 (Figure 4). More dramatic changes to the hydroxyl group that increase the steric bulk can reduce potency by 1000-fold or more (Sjogen, 1995). The portion of the active site that surrounds the phenolic hydroxyl group is tightly packed and cannot accommodate additional atoms. Significant variations in potency are also seen in MPA analogs that alter the hexenoic acid side chain. Reduction of the carboxylate group to the alcohol, or esterification, leads to a 50-fold reduction in IMPDH inhibition (D. Armistead, unpublished data). These changes would interfere with hydrogen bonding to Ser-276. Examples of constrained side-chain compounds that are more potent in vitro IMPDH inhibitors than MPA have been disclosed (Artis et al., 1995). Ab initio and molecular dynamics calculations indicate that many of these analogs have low-energy conformations that preserve the hydrogen bonds with Ser-276 while reducing the entropy of the hexenoic acid side chain.

Similarity of IMPDH to Other Enzymes

Insight into the structure and mechanism of related enzymes is revealed in part by the IMPDH structure. Sequence database searching identified GMP reductase as the closest IMPDH homolog, with 63% similarity and 37% identity over a region of 150 amino acids that included the active-site cysteine as well as the phosphate binding site. The high level of sequence conservation around the active site suggests that GMP reductase has a similar fold and active-site geometry to IMPDH. This is supported by the observation that GMP reductase, like IMPDH, binds substrate before cofactor (Spector et al., 1979).

The structure of the IMPDH α/β barrel is similar to that of other flavin and nicotinamide-dependent oxidoreductases, including glycolate oxidase, the NADPH-dependent aldo-keto reductases, and triethylamine dehydrogenase. The C-terminally sequence-encoded phosphate-binding site is also conserved, but in IMPDH this site is occupied by the IMP ribose phosphate, rather than by the phosphates of the flavin or nicotinamide adenine dinucleotide phosphate (NADP) cofactors as seen in the other enzymes. This suggests that the NAD binding site in IMPDH is novel and may help explain the specificity seen with inhibitors that bind in this site, such as MPA and thiazole adenine dinucleotide (Lee et al., 1985; Hedstrom and Wang, 1990). In contrast, nucleoside analog inhibitors that are competitive with IMP, such as mizoribine and ribavirin phosphate, are more likely to recognize the consensus nucleotide phosphate-binding site found in other enzymes and are thus likely to be less specific than MPA.

Conclusion

We have determined the high resolution crystal structure of IMPDH in complex with an IMP reaction intermediate (XMP*) and MPA. IMPDH is a key enzyme in the de novo pathway of purine biosynthesis in B and T cells, and MPA is the active metabolite of a recently approved immunosuppressive drug. The structure reveals atomic level details of the enzymatic mechanism of IMPDH and the nature of the inhibition of IMPDH by MPA. The active site contains an IMP intermediate covalently linked to Cys-331, which confirms the correct enzymatic mechanism for IMPDH. The structure also indicates that MPA inhibits the enzyme by simultaneously mimicking the nicotinamide portion of the NAD cofactor and a catalytic water molecule. We observe K^+ ion bound near the active site and tetramer interface, which explains the dependence on this cation for enzyme activity. Further, we find that IMPDH contains a unique phosphate-binding site, which reveals in part the specificity of MPA for IMPDH versus other NAD-binding enzymes.

The structural information should facilitate the development of more efficacious IMPDH inhibitors that address the limitations of MPA. Mycophenolate mofetil (CellCept™), a prodrug of MPA which quickly liberates free MPA in vivo, is an effective immunosuppressant available for the prevention of rejection following kidney transplantation (Shaw et al., 1995; Sollinger, 1995). Several clinical observations, however, limit the therapeutic potential of this drug (Shaw et al., 1995). MPA is rapidly metabolized to the glucuronide in vivo, which then undergoes enterohepatic recycling (Allison and Eugui, 1993). This metabolic profile leads to accumulation of drug substance in the gastrointestinal tract (Shaw et al., 1995; P. Chaturvedi, unpublished data), thereby lowering the in vivo potency and contributing to gastrointestinal side effects. Novel IMPDH inhibitors designed in part from the structural information presented here may result in improved therapeutics for use in cancer and immunosuppressive chemotherapy.

Experimental Procedures

Crystallization and Data Collection

Details of sample preparation for crystallization are described elsewhere (Fleming et al., 1996). Crystals of inhibited Chinese hamster IMPDH were grown by vapor diffusion when protein (20 mg ml^{-1} in 300 mM KCl, 10% glycerol, 2 mM MPA, 2 mM 2-mercaptoethanol, 2 mM EDTA, 50 mM Tris [pH 8.0]) was mixed with reservoir (10% polyethylene glycol 6K, 1 M LiCl, 100 mM morpholinoethyl sulfonic acid, 5% 1-methyl-2-pyrrolidinone [v/v], 40 mM 2-mercaptoethanol [pH 5.8]) at a 4:2 ratio and allowed to stand over the reservoir solution at 22°C. Crystals were equilibrated using reservoir solution plus 9% glycerol and 2 mM MPA prior to heavy atom derivitization and then cryoprotected with reservoir solution plus 15% glycerol just before X-ray data collection at −165°C. All data were collected on R-AXIS IIC imaging plates and processed using the software of the manufacturer (Molecular Structure Corp.). The crystals belong to space group P4, with unit cell dimensions $a = b = 110.6$ Å, $c = 111.0$ Å, and angles $\alpha = \beta = \gamma = 90°$. There are two IMDPH monomers per asymmetric unit.

Phasing, Model Building, and Refinement

The structure was determined at 4.0 Å resolution by multiple isomorphous replacement, using data from nine heavy-atom derivatives. The program PHASES (Furey and Swaminathan, 1996) was used for all heavy-atom parameter refinement, multiple isomorphous replacement phasing, solvent flattening, and phase combination. Owing to overlap of heavy atom sites between derivatives and a sharp increase in nonisomorphism, data beyond 4 Å was not helpful for initial multiple isomorphous replacement phasing. The overall mean figure of merit to 4.00 Å resolution was 0.79. Cycles of model building (Quanta 4.1, Molecular Simulations), solvent flattening, phase combination, and phase extension, along with positional refinement (Brunger, 1993), simulated annealing, and torsional dynamics (Rice and Brunger, 1994), were used to complete refinement of the structure. Although the presence of the subdomain (residues 110–244) in the crystals has been confirmed by gel analysis, electron density

for this region remains poor, particularly for one of the two molecules in the asymmetric unit. The current model contains IMPDH residues 11–120, 178–420 (233–420 for the less well-ordered molecule), and 437–514, as well as 202 solvent molecules, two potassium ions, two IMP thioimidates, and two MPA molecules. The R-factor is 21.7% against all observed data (36069 reflections) between 8.0–2.6 Å resolution. The free R value is 28.5% for 3617 reflections set aside at the start of the refinement. Atomic coordinates for IMPDH will be submitted to the Brookhaven Protein Data Bank for release 1 year from the date of publication of this manuscript.

Mutagenesis, Measurement of Specific Activity

Mutations were made in the human type II IMPDH cDNA cloned into a pT7 blue vector (Novagen) by a four-primer polymerase chain reaction (PCR) method (Rashchian et al., 1992) using Pfu DNA polymerase (Stratagen). PCR products were digested with appropriate restriction enzymes and cloned into unique sites within IMPDH cDNA. Mutants were sequenced in the area containing PCR products and the surrounding restriction sites. The full-length IMPDH cDNA carrying the confirmed mutation was then subcloned into a pSPC27 vector in the IMPDH deficient Escherichia coli strain H712 (Nijkamp and Haan, 1967). 500 ml cultures were grown at 37°C for 14–16 hr after isopropyl-β-D-thiogalactopyranoside induction and typically yielded 2 g of cell paste. Cells were resuspended in 50 mM Tris (pH 8.0), 150 mM KCl, 3 mM EDTA, 2 mM dithiothreitol buffer containing 10% urea, and then lysed by addition of lysozyme (1 mg/g cell paste) and sonication. IMPDH wild-type and mutant proteins were precipitated from crude lysates by 25% w/v ammonium sulfate. Up to 150 mg of at least 65%–70% pure IMPDH was obtained by this single purification step. The partially purified IMPDH was resuspended in 50 mM Tris (pH 8.0), 100 mM KCl, 3 mM EDTA, 2 mM dithiothreitol, 10% glycerol buffer and used for kinetic analysis.

Acknowledgments

Correspondence should be addressed to either M. D. S. or K. P. W. We thank David Livingston for critical reading of the manuscript and discussions on the mechanism of IMPDH; David Armistead and Jeff Saunders for leadership in the IMPDH program at Vertex; John Fulghum for assistance with fermentation; Lizbeth Hedstrom for samples of human type I and II IMPDH; Maureen DeCenzo for enzyme characterization; Cameron Stuver for kinetic analysis; Elmar Nimmesgern for additional protein purification and proteolytic analysis; Steve Ronkin for synthesis of heavy atom–containing analogs of MPA; Mike Carson, Tom Oldfield, Rod Hubbard, and Axel Brunger for providing prerelease versions of Ribbons 2.6, Quanta 4.2, and X-PLOR 4.0; Manuel Navia for continuous advice and support; and Joe Kim, John Thomson, Vicki Sato, and Joshua Boger for particularly helpful comments on the manuscript.

Received April 3, 1996; revised April 18, 1996.

References

Allison, A.C., Hovi, T., Watts, R.W.E., and Webster, A.D.B. (1975). Immunological observations on patients with Lesch–Nyhan syndrome and on the role of de novo purine synthesis in lymphocyte transformation. Lancet *2*, 1179–1182.

Allison, A.C., Hovi, T., Watts, R.W.E., and Webster, A.D.B. (1977). The role of de novo purine synthesis in lymphocyte transformation. Ciba Foundation Symp. *48*, 207.

Allison, A.C., and Eugui, E.M. (1993). Immunosuppressive and other effects of mycophenolic acid and an ester prodrug, mycophenolate mofetil. Immunol. Rev. *136*, 5–28.

Andrews, S.C., and Guest, J.R. (1988). Nucleotide sequence of the gene encoding the GMP reductase of *Escherichia coli* K12. Biochem. J. *255*, 35–43.

Antonino, L.C., Straub, K., and Wu, J.C. (1994). Probing the active site of human IMP dehydrogenase using halogenated purine riboside 5-monophosphates and covalent modification reagents. Biochemistry *33*, 1760–1765.

Artis, D.R., Elworthy, T.R., Hawley, R.C., Loughhead, D.G., Morgans, D.J., Jr., Nelson, P.H., Patterson, J.W., Jr., Rohloff, J.C., Sjogren, E.B., Smith, D.B., Waltos, A.M., Weikert, R.J., Garcia, A.C., Zertuche, M.F., Andrade, F.F., Hernandez, M.T.L., Murra, F.X.T., and Martin, T.A.T. (1995). 5-Substituted Derivatives of Mycophenolic Acid. World Patent WO 95/22538.

Blundell, T.L., and Johnson, L.N. (1976). Protein Crystallography (New York: Academic Press).

Bork, P., Gellerich, J., Groth, H., Hooft, R., and Martin, F. (1995). Divergent evolution of a β/α barrel subclass: detection of numerous phosphate-binding sites by motif search. Protein Sci. *4*, 268–274.

Brunger, A.T. (1993). X-PLOR: A System for X-Ray Crystallography and NMR (New Haven, Connecticut: Department of Molecular Biophysics and Biochemistry, Yale University).

Carr, S.F., Papp, E., Wu, J.C., and Natsumeda, Y. (1993). Characterization of human type I and type II IMP dehydrogenases. J. Biol. Chem. *268*, 27286–27290.

Carson, M. (1991). Ribbons 2.0. J. Appl. Cryst. *24*, 958–961.

Collart, F.R., and Hubermann, E. (1988). Cloning and sequence analysis of the human and Chinese hamster inosine-5′-monophosphate dehydrogenase cDNAs. J. Biol. Chem. *263*, 15769–15772.

Collart, F.R., and Hubermann, E. (1990). Expression of IMP dehydrogenase in differentiating HL-60 cells. Blood *75*, 570–576.

Collart, F.R., Chubb, C.B., Mirkin, B.L., and Huberman, E. (1992). Increased inosine-5-monophosphate dehydrogenase gene expression in solid tumor tissues and tumor cell lines. Cancer Res. *52*, 5826–5828.

Cooney, D., Hamel, E., Cohen, M., Kang, G.J., Dalal, M., and Marquez, V. (1987). A simple method for the rapid determination of the stereospecificity of NAD-dependent dehydrogenases applied to mammalian IMP dehydrogenase and bacterial NADH peroxidase. Biochim. Biophys. Acta *916*, 89–93.

Crabtree, G.W., and Henderson, J.F. (1971). Rate-limiting steps in the interconversion of purine ribonucleotides in Ehrlich ascites tumor cells in vitro. Cancer Res. *31*, 985–991.

Dayton, J.S., Lindsten, R., Thompson, C.B., and Mitchell, B.S. (1994). Effects of human T lymphocyte activation on inosine monophosphate dehydrogenase expression. J. Immunol. *152*, 984–991.

Fleming, M.A., Chambers, S.P., Connelly, P.R., Nimmesgern, E., Fox, T., Bruzzese, F.J., Hoe, S.T., Fulghum, J.R., Livingston, D.J., Stuver, C.M., Sintchak, M.D., Wilson, K.P., and Thomson, J.A. (1996). Inhibition of IMPDH by mycophenolic acid: dissection of forward and reverse pathways using capillary electrophoresis. Biochemistry, in press.

Furey, W., and Swaminathan, S. (1996). PHASES-95: a program package for the processing and analysis of diffraction data from macromolecules. In Macromolecular Crystallography: A Volume of Methods in Enzymology, C. Carter and R. Sweet, eds. (Orlando, Florida: Academic Press), in press.

Franklin, T.J., and Cook, J.M. (1969). The inhibition of nucleic acid synthesis by mycophenolic acid. Biochem. J. *113*, 515–524.

Giblett, E.R., Anderson, J.E., Cohen, F., and Meuwissen, H.J. (1972). Adenosine deaminase deficiency in two patients with severely impaired cellular immunity. Lancet *2*, 1067.

Gosio, B. (1896). Riv. Igiene Sanita Pubbl. Ann. *7*, 825.

Hager, P.W., Collart, F.R., Huberman, E., and Mitchell, B.S. (1995). Recombinant human inosine monophosphate dehydrogenase type I and type II proteins: purification and characterization of inhibitor binding. Biochem. Pharmacol. *49*, 1323–1329.

Harrison, W., Shearer, M.M., and Trotter, J. (1972). Crystal structure of mycophenolic acid. J. Chem. Soc., Perkin Trans. *2*, 1542–1544.

Hedstrom, L., and Wang, C.C. (1990). Mycophenolic acid and thiazole adenine dinucleotide inhibition of Tritrichomonas foetus inosine 5′-monophosphate dehydrogenase: immplication on enzyme mechanism. Biochemistry *29*, 849–854.

Hodges, S.D., Fung, E., McKay, D.J., Renaux, B.S., and Snyder, F.F. (1989). Increased activity, amount, and altered kinetic properties of IMP dehydrogenase from mycophenolic acid-resistant neuroblastoma cells. J. Biol. Chem. *264*, 18137.

Holm, L., and Sander, C. (1996). Protein structure comparison by alignment of distance matrices. Nucl. Acids Res. *24*, 206–209.

Holmes, E.W., Pehlke, D.M., and Kelley, W.N. (1974). Human IMP dehydrogenase: kinetics and regulatory properties. Biochim. Biophys. Acta *364*, 209–217.

Huete-Perez, J.A., Wu, J.C., Whitby, F.G., and Wang, C.C. (1995). Identification of the IMP binding site in the IMP dehydrogenase from Tritrichomonas foetus. Biochemistry *34*, 13889–13894.

Jackson, R.C.B., Weber, G., and Harris, H.P. (1975). IMP dehydrogenase, an enzyme linked with proliferation and malignancy. Nature *256*, 331–333.

Kabsch, W., and Sander, C. (1983). Dictionary of protein secondary structure: pattern recognition of hydrogen-bonded and geometrical features. Biopolymers *22*, 2577–2637.

Konno, Y., Natsumeda, Y., Nagai, M., Yamaji, Y., Ohno, S., Suzuki, K. and Weber, G. (1991). Expression of human IMP dehydrogenase types I and II in *Escherichia coli* and distribution in human normal lymphocytes and leukemic cell lines. J. Biol. Chem. *266*, 506–509.

Lee, H.J., Pawlak, K., Nguyen, B.T., Robins, R.K., and Sadee, W. (1985). Biochemical differences among four inosinate dehydrogenase inhibitors, mycophenolic acid, ribavirin, tiazofurin, and selenazofurin, studied in mouse lymphoma cell culture. Cancer Res. *45*, 5512–5520.

Lightfoot, T., and Synder, F.F. (1994). Gene amplification and dual point mutations of mouse IMP dehydrogenase associated with cellular resistance to mycophenolic acid. Biochem. Biophys. Acta *1217*, 156–162.

Link, J.O., and Straub, K., (1996). Trapping of an IMP dehydrogenase–substrate covalent intermediate by mycophenolic acid. J. Am. Chem. Soc. *118*, 2091–2092.

Makara, G.M., Keseru, G.M., Kajtar-Peredy, M., and Anderson, W.K. (1996). Nuclear magnetic resonance and molecular modeling study on mycophenolic acid: implications for binding to inosine monophosphate dehydrogenase. J. Med. Chem. *39*, 1236–1242.

Morrison, J.F. (1969). Kinetics of the reversible inhibition of enzyme-catalyzed reactions by tight-binding inhibitors. Biochem. Biophys. Acta *185*, 269–286.

Nagai, M., Natsumeda, Y., Konno, Y., Hoffman, R., Irino, S., and Weber, G. (1991). Selective up-regulation of type II inosine 5′-monophosphate dehydrogenase messenger RNA expression in human leukemias. Cancer Res. *51*, 3886–3890.

Nagai, M., Natsumeda, Y., and Weber, G. (1992). Proliferation-linked regulation of type II IMP dehydrogenase gene in human normal lymphocytes and HL-60 leukemic cells. Cancer Res. *52*, 258–261.

Nakamura, H., Natsumeda, Y., Nagai, M., Takahara, J., Irino, S., and Weber, G. (1992). Reciprocal alterations of GMP reductase and IMP dehydrogenase activities during differentiation in HL-60 leukemia cells. Leukemia Res. *16*, 561–564.

Natsumeda, Y., Ikegami, T., Murayama, K., and Weber, G. (1988). *De novo* guanylate synthese in the commitment to replication in hepatoma 3924A cells. Cancer Res. *48*, 507–511.

Natsumeda, Y., Ohno, S., Kawasaki, H., Konno, Y., Weber, G., and Suzuki, K. (1990). Two distinct cDNAs for human IMP dehydrogenase. J. Biol. Chem. *265*, 5292–5295.

Natsumeda, Y., and Carr, S.F. (1993). Human type I and II IMP dehydrogenases as drug targets. Ann. NY Acad. Sci. *696*, 88–93.

Nijkamp, H.J.J., and Haan, P.G. (1967). Genetic and biochemical studies of the guanosine-5′-monophosphate pathway in *Escherichia coli*. Biochem. Biophys. Acta *145*, 31–40.

Rashchian, A., Thornton, C.G., and Heidecker, G. (1992). A novel method for site-directed mutagenesis using PCR and uracil DNA glycosylase. PCR Meth. Applic. *2*, 124–130.

Read, R.J. (1986). Improved Fourier coefficients for maps using phases from partial structures with errors. Acta Cryst. *A42*, 140–149.

Rice, L.M., and Brunger, A.T. (1994). Torsion angle dynamics: reduced variable conformational sampling enhances crystallographic structure refinement. Protein Struct. Funct. Genet. *19*, 277–290.

Senda, M., and Natsumeda, Y. (1994). Tissue-differential expression of two distinct genes for human IMP dehydrogenase. Life Sci. *54*, 1917–1926.

Shaw, L.M., Sollinger, H.W., Halloran, P., Morris, R.E., Yatscoff, R.W., Ransom, J., Tsina, I., Keown, P., Holt, D.W., Lieberman, R., Jaklitsch, A., and Potter, J. (1995). Mycophenolate mofetil: a report of the consensus panel. Therapeut. Drug Monitor. *17*, 690–699.

Sjogen, E.B. (1995). 4-Amino Derivatives of Mycophenolic Acid with Immunosuppressant Activity. World Patent WO 95/22535.

Snyder, F.F., Henderson, J.F., and Cook, D.A. (1972). Inhibition of purine metabolism: computer-assisted analysis of drug effects. Biochem. Pharmacol. *21*, 2351–2357.

Sollinger, H.W. (1995). Mycophenolate mofetil for the prevention of acute rejection in primary cadaveric renal allograft recipients (US Renal Transplant Mycophenolate Mofetil Study Group). Transplantation *60*, 225–232.

Spector, T., Jones, T.E., and Miller, R.L. (1979). Reaction mechanism and specificity of human GMP reductase: substrates, inhibitors, activators, and inactivators. J. Biol. Chem. *254*, 2308–2315.

Wang, W., Papov, V.V., Minakawa, N., Matsuda, A., Biemann, K., and Hedstrom, L. (1996). Inactivation of inosine 5′-monophosphate dehydrogenase by the antiviral agent 5-ethynyl-1-β-D-ribofuranosylimidazole-4-carboxamide 5′-monophosphate. Biochemistry *35*, 95–101.

Weber, G. (1983). Biochemical strategy of cancer cells and the design of chemotherapy. Cancer Res. *43*, 3466–3492.

Wolfenden, R., and Kati, W.M. (1991). Testing the limits of protein-ligand binding discrimination with transition-state analogue inhibitors. Acct. Chem. Res. *24*, 209–215.

Wu, Y-D., Lai, D.K.W., and Houk, K.N. (1995). Transition structures of hydride transfer reactions of protonated pyridinium ion with 1,4-dihydropyridine and protonated nicotinamide with 1,4-dihydronicotinamide. J. Am. Chem. Soc. *117*, 4100–4108.

Xiang, B., Taylor, J.C., and Markham, G.D. (1996). Monovalent cation activation and kinetic mechanism of inosine 5′-monophosphate dehydrogenase. J. Biol. Chem. *271*, 1435–1440.